Parametrisation of F_2^γ at low Q^2 and of $\sigma_{\gamma\gamma}$ and $\sigma_{\gamma^*\gamma}$ at high energies

B. Badełek[a], M. Krawczyk[b], J. Kwieciński[c] and A. M. Staśto[c]

[a] *Department of Physics, Uppsala University, P.O.Box 530, 751 21 Uppsala, Sweden and Institute of Experimental Physics, Warsaw University, 00-681 Warsaw, Poland*

[b] *Institute of Theoretical Physics, Warsaw University, 00-681 Warsaw, Poland*

[c] *Department of Theoretical Physics, H. Niewodniczański Institute of Nuclear Physics, 31-342 Cracow, Poland*

Abstract

A parametrisation of the real photon structure function F_2^γ in the low Q^2, low x region is formulated. It includes both the VMD and the QCD components, the latter suitably extrapolated to the low Q^2 region and based on arbitrary parton distributions in the photon. The parametrisation used together with the GRV and GRS' parton densities describes reasonably well the existing high energy data on F_2^γ, $\sigma_{\gamma\gamma}$ and the low Q^2 data on $\sigma_{\gamma^*\gamma}$. Predictions for $\sigma_{\gamma\gamma}$ and for $\sigma_{\gamma^*\gamma}$ for energies which may become accessible in future linear colliders are also given.

1 Introduction

Electron–photon scattering,

$$e\,\gamma \to \gamma^*\gamma \to hadrons, \tag{1}$$

studied in high energy e^+e^- collisions with tagged electron is an analogue of the inelastic lepton–nucleon scattering. Here the probe – a virtual photon of four momentum q ($q^2 = -Q^2 < 0$), tests the target particle, the real photon of four momentum p ($p^2 = 0$). The corresponding spin averaged cross section, Fig.1, can be parametrized e.g. by the photon structure functions $F_1^\gamma(x, Q^2)$ and $F_2^\gamma(x, Q^2)$. The Bjorken parameter x is conventionally defined as $x = Q^2/(2p \cdot q)$. Thus the process (1) permits an insight into the inner structure of the real photon.

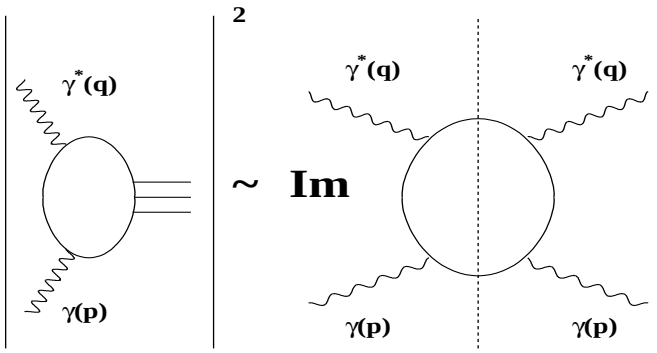

Figure 1: The cross section for the $\gamma^*\gamma \to hadrons$ scattering and its relation to the imaginary part of the forward $\gamma^*\gamma \to \gamma^*\gamma$ amplitude.

At large Q^2 the photon structure function is described by the perturbative QCD [1, 2, 3, 4, 5]. However in the low Q^2 region, $Q^2 \lesssim 1$ GeV^2, it is expected that the Vector Meson Dominance (VMD) contribution [6] is important.

In this paper we present a model of the photon structure function F_2^γ which includes both the VMD contribution and the QCD term, suitably extrapolated to the low Q^2 region. This approach is based on the extension of a similar representation of the nucleon structure function [7, 8, 9] to the case of the photon. Possible parametrisations

of the photon structure function which extend to the low Q^2 region have also been discussed in Ref. [10, 11, 12]. The parametrisation proposed in Ref.[10] is based upon the Quark Parton Model supplemented by the contribution from the hadronic structure of the photon. The energy dependence of the latter has a Regge form. The Q^2 dependence is parametrised in terms of the simple form-factors which if combined with the Regge-type energy dependence generate at large Q^2 the Bjorken scaling behaviour of the corresponding part of the structure function. In Ref. [11] the energy dependence of the cross-section is also parametrised in a Regge-like form with the Q^2 dependence specified by the suitable form factors which contain terms corresponding to the VMD contribution. The parametrisation discussed in [12] is based upon a model corresponding to the interaction of colour dipoles, i.e. the $q\bar{q}$ pairs which the photon(s) fluctuate into. In our approach the contribution coming from the light vector mesons within the Vector Meson Dominance model is similar to that used by other authors (see eg. [11]) although the details concerning estimate of the relevant total cross-sections are slightly different. The novel feature of our model is the treatment of the contribution coming from high masses of the hadronic states which couple to the virtual photons. In our scheme this contribution is directly related to the photon structure function in the large Q^2 region. The low and high mass hadronic states are separated at Q_0, a parameter whose value was taken identical with that for the F_2^p.

Our framework permits to describe the $\gamma\gamma$ and $\gamma^*\gamma$ total cross sections as functions of energy. The energy dependence of $\sigma_{\gamma\gamma}$ is also described by other models, [11, 12, 13, 14, 15, 16, 17, 18]. Most of them incorporate the Regge-like parametrisation of the total $\gamma\gamma$ cross-sections; some provide a detailed insight into the structure of final states and a decomposition of the $\gamma\gamma$ total cross-section into terms corresponding to the appropriate subdivision of photon interactions and event classes [11, 14]. Possibility that part of the $\gamma\gamma$ cross-section is driven by the production of minijets has been discussed in [13, 16]. Certain approaches analyse the behaviour of the cross-sections on the virtualities of both interacting photons [11, 12, 15, 17, 18].

The content of our paper is as follows: In the next section we recall the QCD description of the photon structure functions and in section 3 we briefly describe the Vector Meson Dominance model in the process $\gamma^*\gamma \to hadrons$. In section 4 we present a parametrisation of the photon structure function, as well as the total cross section for the interaction of two real photons and of the virtual and real photon. In section 5 we compare our theoretical predictions with the experimental data on the F_2^γ and on the total cross sections $\sigma_{\gamma\gamma}$ and $\sigma_{\gamma^*\gamma}$. We also give predictions for $\sigma_{\gamma\gamma}$ in the very high energy range which can become accessible in future linear colliders. Finally in section 6 we give the summary of our results.

2 Partonic content of the photon

In the large Q^2, i.e. in the deep inelastic limit the virtual photon probes the quark (antiquark) structure of the (real) photon in analogy to the deep inelastic lepton–hadron scattering, Fig.2. The corresponding photon structure function $F_2^\gamma(x, Q^2)$ may

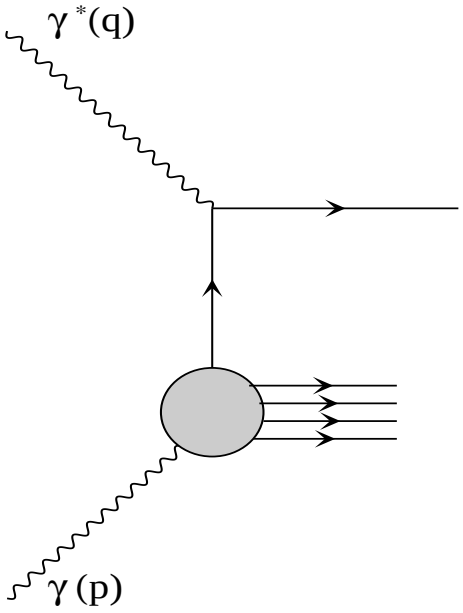

Figure 2: $\gamma^*\gamma$ scattering as a mechanism for probing partonic structure of the real photon

thus be related to quark and antiquark distributions $q_i^\gamma(x, Q^2)$, $\overline{q}_i^\gamma(x, Q^2)$ in the photon:

$$F_2^\gamma(x, Q^2) = \; x \sum_i \; e_i^2 \; [\; q_i^\gamma(x, Q^2) \; + \; \bar{q}_i^\gamma(x, Q^2)], \tag{2}$$

where e_i denote the charges of quarks and antiquarks and the sum is over all active quark flavours. To be precise equation (2) holds in leading logarithmic approximation of perturbative QCD. It acquires higher order corrections in next-to-leading approximation and beyond [19, 20].

A special feature of the quark structure of the photon with respect to the proton is a possibility of a direct $q\bar{q}$ production through the process $\gamma^*\gamma \to q\bar{q}$, see Fig.3, leading to the parton model predictions for the $q_i^\gamma(x, Q^2)$ and $\bar{q}_i^\gamma(x, Q^2)$. A contribution of this process introduces an inhomogeneous term into the equation describing the QCD evolution of the quark (and antiquark) distributions in the photon. The process $\gamma^*\gamma \to q\bar{q}$ (modified by the QCD evolution) with the pointlike quark coupling both to real and virtual photons dominates in the large Q^2 limit making the photon structure functions exactly calculable in this limit [1, 2]. Striking features of these functions are:

- $F_{1,2}^\gamma$ rise with increasing x at large x;

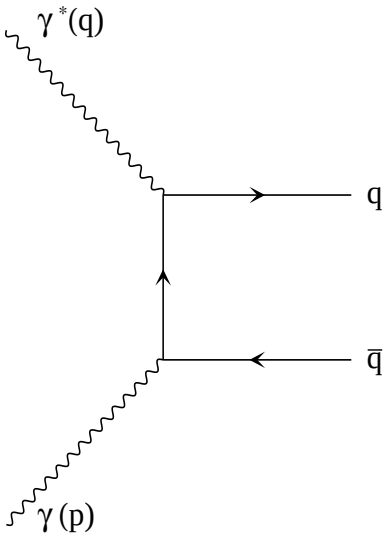

Figure 3: Diagrammatic representation of the direct $\gamma^*\gamma \to q\bar{q}$ process.

- $F_{1,2}^{\gamma}$ show the scaling violation, $F_{1,2}^{\gamma} \sim \ln Q^2$.

At low values of x the dominant role in the photon structure functions is played by gluons. The situation here is similar to that of the hadronic structure functions which exhibit a very strong increase with decreasing x, see e.g. [21]. Those effects are still rather weak in the kinematical region of F_2^{γ} probed by present experiments but they will be very important in the regime accessible in the future linear e^+e^- ($e\gamma$, $\gamma\gamma$) colliders [22].

Besides the direct, point-like coupling to quarks, the target photon can fluctuate into vector mesons and other hadronic states which can also have their partonic structure. The latter cannot be calculated perturbatively and thus has to be parametrised phenomenologically [23].

Finally it should be pointed out that the charm quark playing the dominant role in the heavy quark contributions to $F_2^{\gamma}(x, Q^2)$, is often described just by the lowest order Bethe-Heitler cross-section for the process $\gamma^*\gamma \to c\bar{c}$ and the additional contribution generated by the radiation $g \to c\bar{c}$ [20, 23].

3 Dispersive relation for $\gamma^*\gamma$ scattering. F_2^{VMD} and $F_2^{partons}$ contributions to F_2^{γ}

The QCD describes the photon structure functions in the large Q^2 region. In the low Q^2 region however one expects that the VMD mechanism is important. By the Vector

Meson Dominance mechanism in this case we understand the model in which the virtual photon of virtuality Q^2 fluctuates into vector mesons which next undergo interaction with the (real) photon of virtuality $p^2 \simeq 0$, see Fig.4. In order to be able to describe the photon structure function for arbitrary values of Q^2 it would be very useful to have a unifed scheme which contains both the VMD and the QCD contributions, the latter suitably extended to the region of low values of Q^2. This may be achieved by utilising

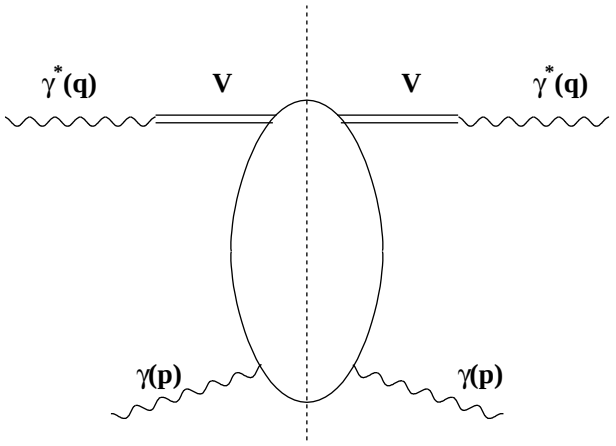

Figure 4: Diagrammatic repesentation of the Vector Meson Dominance model in the $\gamma^*\gamma$ scattering.

the dispersive representation in Q^2 of the structure function. To this aim let us notice that the $\gamma^*\gamma$ collision can be viewed as the interaction of a real photon target with a photon with virtuality Q^2 which fluctuates onto general hadronic state, cf. Fig.5. We consider the virtual photon first fluctuating onto the $q\bar{q}$ state and then interacting with the real photon. Like in the γ^*p scattering one can write the dispersion relation for the $\gamma^*\gamma$ scattering as follows [6]:

$$F_2^\gamma(W^2, Q^2) =$$

$$\frac{Q^2}{4\pi^2\alpha} \sum_q \int \frac{dM^2}{M^2+Q^2} \int \frac{dM'^2}{M'^2+Q^2} \rho(M^2, M'^2) \frac{1}{W^2} \text{ Im } A_{(q\bar{q})-\gamma}(W^2, M^2, M'^2) \quad (3)$$

where M and M' are the invariant masses of the incoming and outgoing $q\bar{q}$ pair. In eq. (3), $\rho(M^2, M'^2)$ is the density matrix of the $q\bar{q}$ states and $\text{Im}A_{(q\bar{q})-\gamma}$ is an imaginary part of the corresponding forward scattering amplitude.

The above formula can be rewritten in a form of a single dispersion relation as

follows,

$$F_2^\gamma(W^2,Q^2) \;=\; Q^2 \int_0^\infty \frac{dQ'^2}{(Q'^2+Q^2)^2}\,\Phi(W^2,Q'^2) \tag{4}$$

where the spectral function

$$\begin{aligned}\Phi(W^2,Q'^2) \;&=\; \frac{1}{4\pi^2\alpha}\int_0^1 d\lambda \int dM^2 \int dM'^2\,\delta(Q'^2-\lambda M'^2-(1-\lambda)M^2) \\ &\quad \rho(M^2,M'^2)\,\frac{1}{W^2}\,\mathrm{Im}A_{(q\bar{q})-\gamma}(W^2,M^2,M'^2).\end{aligned} \tag{5}$$

The centre-of-mass energy squared $W^2=(p+q)^2$ is related to the Bjorken parameter x in the following way:

$$W^2 \;=\; Q^2(\frac{1}{x}-1). \tag{6}$$

One can now separate regions of low- and high values of Q'^2 in the integral (4), by noticing that this integral corresponds to the (Generalised) Vector Meson Dominance representation of the F_2^γ.

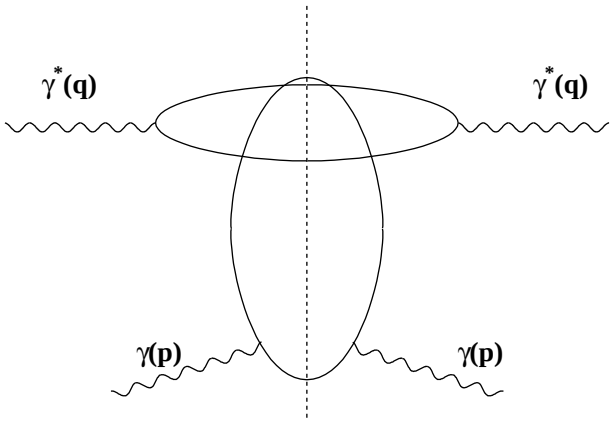

Figure 5: Diagrammatic representation of the dispersion relation.

For low values of Q'^2, $Q'^2 < Q_0^2$, one uses the Vector Meson Dominance model. In this approach one assumes that the virtual photon forms a vector meson rather than a pair of well separated q and $\bar{q}$. The integrand in the integral on the right hand side of

equation (5) defining the spectral function $\Phi(W^2, Q'^2)$ is then given by the following formula:

$$\rho(M^2, M'^2)\,\frac{1}{W^2}\,\mathrm{Im}A_{(q\bar{q})-\gamma}(W^2, M^2, M'^2)$$
$$= \pi\alpha \sum_V \frac{M_V^4}{\gamma_V^2}\sigma_{V\gamma}\,(W^2)\delta(M^2 - M_V^2)\delta(M'^2 - M_V^2), \tag{7}$$

where M_V is the mass of the vector meson V and $\sigma_{V\gamma}(W^2)$ denotes the $V\gamma$ total cross section. The couplings γ_V^2 can be estimated from the leptonic widths of the vector mesons,

$$\frac{\gamma_V^2}{\pi} = \frac{\alpha^2 M_V}{3\Gamma^V_{e^+e^-}}\ . \tag{8}$$

In equation (7) we have included only diagonal transitions between the vector mesons having the same masses. The corresponding spectral function $\Phi^{VMD}(W^2, Q'^2)$ thus reads:

$$\Phi^{VMD}(W^2, Q'^2) = \sum_V \frac{M_V^4}{4\pi\gamma_V^2}\sigma_{V\gamma}\,(W^2)\delta(Q'^2 - M_V^2). \tag{9}$$

The resulting VMD contribution to the photon structure function F_2^γ , F_2^{VMD}, is given by the following equation:

$$F_2^{\mathrm{VMD}}(x, Q^2)\ =\ \frac{Q^2}{4\pi}\ \sum_V\ \frac{M_V^4\ \sigma_{V\gamma}\,(W^2)}{\gamma_V^2(Q^2 + M_V^2)^2}\ . \tag{10}$$

In eq.(10) we only consider mesons with masses $M_V^2 < Q_0^2$. The contribution coming from the region of high values of Q'^2 ($Q'^2 > Q_0^2$) can be related to the photon structure function from the large Q^2 domain. It defines the partonic contribution F_2^{partons} to the structure function F_2^γ, extended to arbitrary low values of Q^2. For convenience, we adopt the approximation used in Ref. [8] which gives:

$$F_2^{\mathrm{partons}}(x, Q^2)\ =\ \frac{Q^2}{Q^2 + Q_0^2}\ F_2^{\mathrm{QCD}}(\bar{x}, Q^2 + Q_0^2) \tag{11}$$

where

$$\bar{x}\ =\ \frac{Q^2 + Q_0^2}{W^2 + Q^2 + Q_0^2}\ . \tag{12}$$

The structure function F_2^{QCD} is taken from the QCD analysis, valid in the large Q^2 region, i.e. it is calculated from the existing parametrisations of the parton distributions. Modifications of the QCD contribution: replacement of the parameter x by $\bar{x}$ defined in equation (12), shift of the scale $Q^2 \to Q^2 + Q_0^2$ and the factor $Q^2/(Q^2 + Q_0^2)$ instead of 1, introduce power corrections which vanish as $1/Q^2$ and are negligible at large Q^2. The magnitude of Q_0^2 is set to 1.2 GeV^2 as in the case of the proton [7, 8]. The F_2^{partons} thus defines a contribution to F_2^γ at arbitrary low values of Q^2.

An elaborated treatment of the partonic contribution to the proton structure function has been developed in Ref. [9], where long and short distance components have been carefully separated. According to that paper the low mass region is dominated by the $q\bar{q}$ pairs with large transverse sizes in the impact parameter space (thus corresponding to the VMD) whereas the QCD part is dominated by pairs of small transverse size.

4 Parametrisation of the photon structure function and of the total photon–photon interaction cross sections

Our representation of the photon structure function $F_2^\gamma(x,Q^2)$ is based on the following decomposition:

$$F_2^\gamma(x,Q^2) = F_2^{\rm VMD}(x,Q^2) + F_2^{\rm partons}(x,Q^2) \tag{13}$$

where $F_2^{\rm VMD}$ and $F_2^{\rm partons}(x,Q^2)$ are defined by eq. (10) and (11). A total $\gamma^*\gamma$ cross-section in the high energy limit is given by

$$\sigma_{\gamma^*\gamma}(W,Q^2) = \frac{4\pi^2\alpha}{Q^2} F_2^\gamma(x,Q^2), \tag{14}$$

with $x = Q^2/(Q^2+W^2)$. The $Q^2 = 0$ (for fixed W) limit of eq. (14) gives the total cross-section $\sigma_{\gamma\gamma}(W^2)$ corresponding to the interaction of two real photons. ¿From (13), (10) and (11) we obtain the following expression for this cross-section at high energy:

$$\sigma_{\gamma\gamma}(W) = \alpha\pi \sum_{V=\rho,\omega,\phi} \frac{\sigma_{V\gamma}(W^2)}{\gamma_V^2} + \frac{4\pi^2\alpha}{Q_0^2} F_2^{\rm QCD}(Q_0^2/W^2, Q_0^2)\ . \tag{15}$$

At large Q^2 the structure function given by eq. (13) becomes equal to the QCD contribution $F_2^{\rm QCD}(x,Q^2)$. The VMD component gives the power correction term which vanishes as $1/Q^2$ for large Q^2. It should be noted that the VMD part contains only finite number of vector mesons with their masses smaller than Q_0^2.

In the quantitive analysis of the photon structure function and of the total cross sections we have taken the structure function $F_2^{\rm QCD}$ from the LO analyses presented in Ref. [19] (GRV) and [20] (GRS'),with a number of active flavours equal four. The latter parton parametrization is based on updated data analysis and holds for both virtual and real photons.

The VMD part was estimated using the following assumptions:

1. Numerical values of the couplings γ_V^2 are the same as those used in Ref. [7]. They were estimated from the relation (8) which gives the following values:

$$\frac{\gamma_\rho^2}{\pi} = 1.98, \qquad \frac{\gamma_\omega^2}{\pi} = 21.07, \qquad \frac{\gamma_\phi^2}{\pi} = 13.83. \tag{16}$$

2. Cross-sections $\sigma_{V\gamma}$ are represented as sums of the Pomeron and Reggeon contributions:

$$\sigma_{V\gamma}(W^2) = P_{V\gamma}(W^2) + R_{V\gamma}(W^2) \tag{17}$$

where

$$P_{V\gamma}(W^2) = a_{V\gamma}^P \left(\frac{W^2}{W_0^2}\right)^{\lambda_P} \tag{18}$$

$$R_{V\gamma}(W^2) = a_{V\gamma}^R \left(\frac{W^2}{W_0^2}\right)^{\lambda_R} \tag{19}$$

with

$$\lambda_R = -0.4525, \qquad \lambda_P = 0.0808 \tag{20}$$

and W_0^2 =1 GeV^2 [24].

3. Pomeron couplings $a_{V\gamma}^P$ are related to the corresponding couplings $a_{\gamma p}^P$ controlling the Pomeron contributions to the total γp cross-sections. We assume the additive quark model and reduce the total cross-sections for the interaction of strange quarks by a factor 2. This gives:

$$a_{\rho\gamma}^P = a_{\omega\gamma}^P = \frac{2}{3} a_{\gamma p}^P \ ,$$

$$a_{\phi\gamma}^P = \frac{1}{2} a_{\rho\gamma}^P \ . \tag{21}$$

4. Reggeon couplings $a_{V\gamma}^R$ are estimated assuming the additive quark model and the duality (i.e. a dominance of planar quark diagrams). We also assume that the quark couplings to a photon are proportional to the quark charge with the flavour independent proportionality factor. This gives:

$$a_{\rho\gamma}^R = a_{\omega\gamma}^R = \frac{5}{9} a_{\gamma p}^R \ ,$$

$$a_{\phi\gamma}^R = 0 \ . \tag{22}$$

5. Couplings $a^P_{\gamma p}$ and $a^R_{\gamma p}$ are taken from the fit discussed in Ref. [24] which gave:

$$a^R_{\gamma p} = 0.129 \text{ mb}, \qquad a^P_{\gamma p} = 0.0677 \text{ mb} \tag{23}$$

Since we are using the Regge description of total cross sections $\sigma_{V\gamma}(W)$ our approach can only work for large values of W, $W^2 \gtrsim 2$ GeV^2, away from the resonance region.

5 Numerical results

In this section we compare our results for the real photon structure function $F_2^\gamma(x, Q^2)$ and the two-photon cross sections, $\sigma_{\gamma\gamma}(W)$ and $\sigma_{\gamma^*\gamma}(W)$ with corresponding measurements. In some cases our predictions have been extended to the region $W^2 < 2$ GeV^2 where the model may not be applicable. Theoretical curves were obtained using two different parametrisations for the structure function $F_2^{\rm QCD}$, GRV [19] and GRS' [20].

In Fig.6 we show predictions for the photon structure function based on equation (13) plotted as the function of x for different values of Q^2 in the region of small Q^2. In Fig.7 the Q^2 dependence of the photon structure function for different values of x is presented [1]. We confront our theoretical results with existing experimental data [25, 26, 27, 28, 29]. Measurements of F_2^γ are scarce, especially for low values of Q^2. However it can be seen that our prediction reproduces well the data independently of the parametrisation (GRV or GRS') of $F_2^{\rm QCD}$ used in the model. Irregular behaviour of the dashed lines observed in Figs 6 and 7 at high values of x is connected with the teatment of the charm contribution to F_2^γ in the GRS' approach.

In Fig.8 we compare our predictions with the data on $\sigma_{\gamma\gamma}(W)$. Theoretical curves were obtained from equation (15). We show experimental points corresponding to the low energy region ($W \lesssim 10$ GeV) [30, 31, 32] and the recent preliminary high energy data obtained by the L3, OPAL and DELPHI collaborations at LEP [33, 34, 35]. The representation (15) for the total $\gamma\gamma$ cross-section describes the data reasonably well. The result of the calculation based on GRS' parametrisation of $F_2^{\rm QCD}$ is slightly higher and has a shallower minimum as compared to that based on GRV parametrisation. Calculations using the latter give a good description of the shape of the energy dependence of the cross section although the overall normalisation seems to be about 15% too large. It should be stressed that our prediction is essentially parameter free. The magnitude of the cross-section is dominated by the VMD component yet the partonic

[1] In both figures the curves are plotted only for $W > 2m_\pi$ which corresponds to the threshold energy in the reaction $\gamma\gamma \to hadrons$.

part is also non-negligible. In particular the latter term is responsible for generating a steeper increase of the total cross-section with increasing W than that embodied in the VMD part which is described by the soft Pomeron contribution. The decrease of the total cross-section with increasing energy in the low W region is controlled by the Reggeon component of the VMD part (see eqs. (17), (19) and (20)) and by the valence part of the partonic contribution.

In Fig.9 we show predictions for the total $\gamma\gamma$ cross-section as a function of the total centre-of-mass energy W in the wide energy range including the energies that might be accessible in the future linear colliders. In this figure we also show a decomposition of $\sigma_{\gamma\gamma}(W^2)$ into its VMD and partonic components (only GRV parametrisation was used in this analysis). At very high energies these two terms exhibit different energy dependence. The VMD part is described by the soft Pomeron contribution which gives the $W^{2\lambda}$ behaviour with $\lambda = 0.0808$, eq. (20). The partonic component increases faster with energy since its energy dependence reflects the increase of $F_2^{\rm QCD}(\bar{x}, Q_0^2)$ with decreasing $\bar{x}$ generated by the QCD evolution [19, 20]. This increase is stronger than that implied by the soft Pomeron exchange. As a result the total $\gamma\gamma$ cross-section, which is the sum of the VMD and partonic components does also exhibit stronger increase with the increasing energy than that of the VMD component. It is however milder than the increase generated by the partonic component alone, at least for $W < 10^3$ GeV. This follows from the fact that in this energy range the magnitude of the cross-section is still dominated by its VMD component. We found that for sufficiently high energies W the total $\gamma\gamma$ cross-section $\sigma_{\gamma\gamma}(W)$ described by eq. (15) can be parametrized by the effective power law dependence, $\sigma_{\gamma\gamma}(W) \sim (W^2)^{\lambda_{eff}}$, with λ_{eff} slowly increasing with energy ($\lambda_{eff} \sim 0.1 - 0.12$ for 30 GeV $< W < 10^3$ GeV).

In Fig.10 we show the $\gamma^*\gamma$ cross section for different bins of the centre-of-mass energy W plotted versus Q^2, the virtuality of the probing photon. Our theoretical predictions based on equation (14) are compared with measurements by the TPC/2γ Collaboration [31] and the agreement between the two is very good. In Fig.11 we show the $\gamma^*\gamma$ cross section for large energies W plotted versus Q^2 (only GRV parametrsation was used here). At medium and large Q^2, $\sigma_{\gamma^*\gamma}$ decreases as $1/Q^2$ (modulo logaritmic corrections) and for very small values ($Q^2 < 10^{-1}$ GeV^2) it exhibits a flattening behaviour.

6 Concluding remarks

We have presented an extension of the representation developed for the nucleon structure function F_2 for arbitrary values of Q^2, [7, 8], onto the structure function of the real photon. This representation includes both the VMD contribution and the QCD component, obtained from the QCD parton parametrisations for the photon, suitably extrapolated to the region of low Q^2. In the Q^2=0 limit the model gives predictions for the total cross section $\sigma_{\gamma\gamma}$ for the interaction of two real photons.

We showed that our framework is fairly successful in describing the experimental data on $\sigma_{\gamma\gamma}(W)$ and on $\sigma_{\gamma^*\gamma}(W, Q^2)$ and on the photon structure function F_2^γ at low Q^2. We also showed that one can naturally explain the fact that the increase of the total $\gamma\gamma$ cross-section with increasing CM energy W is stronger than that implied by soft Pomeron exchange. The calculated total $\gamma\gamma$ cross-section exhibits an approximate power-law increase with increasing energy W, i.e. $\sigma_{\gamma\gamma}(W) \sim (W^2)^{\lambda_{eff}}$ with λ_{eff} slowly increasing with energy: $\lambda_{eff} \sim 0.1 - 0.12$ for 30 GeV $< W <$ 10^3 GeV.

Acknowledgments

This research was partially supported by the Polish State Committee for Scientific Research grants no. 2 P03B 089 13, 2 P03B 014 14, 2 P03B 184 10 and by the EU Fourth Framework Programme "Training and Mobility of Researchers", Network 'Quantum Chromodynamics and the Deep Structure of Elementary Particles', contract FMRX - CT98 - 0194. AMS thanks Foundation for Polish Science for financial support.

References

[1] E. Witten, Nucl.Phys. **B120** (1977) 189.

[2] C. Peterson, T.F. Walsh and P.M. Zerwas, Nucl.Phys. **B174** (1980) 424; P. Zerwas, Phys.Rev. **D10** (1974) 1485.

[3] H. Abramowicz, M. Krawczyk, K. Charchuła, A. Levy and U. Maor, Int. J. Mod. Phys. **A8** (1993) 1005 and references therein.

[4] Report of the Working Group on $\gamma\gamma$ Physics, P. Aurenche and G.A. Schuler (convenors), Proceedings of the Workshop on Physics at LEP2, CERN yellow

report 96-01 and hep-ph/9601317, G. Altarelli , T. Sjöstrand and P. Zwirner (editors).

[5] M. Krawczyk, Acta Phys. Polon. **B28** (1997) 2659; M. Krawczyk, A. Zembrzuski and M. Staszel, hep-ph/9806291; an extended version of this report is in IFT 99-15 and has been submitted to Phys. Rep.;
P. Nisius, hep-ex/9912049.

[6] T.H. Bauer et al., Rev. Mod. Phys. **50** (1978) 261 and references therein.

[7] J. Kwieciński and B. Badełek, Z.Phys. **C43** (1989) 251.

[8] B. Badełek and J. Kwieciński, Phys. Lett. **B295** (1992) 263.

[9] A.D. Martin, M.G. Ryskin and A.M. Stasto, Eur. Phys. J. **C7** (1999) 643; Nucl. Phys. Proc. Suppl. **74** (1999) 121.

[10] E. Gotsman, A. Levy and U. Maor, Z. Phys. **C40** (1988) 117.

[11] G. A. Schuler, Comput. Phys. Commun. **108** (1998) 279.

[12] A. Donnachie , H. G. Dosch and M. Rueter, Phys.Rev. **D59** (1999) 074011.

[13] J.R. Forshaw and J.K. Storrow, Phys. Rev. **D46** (1992) 4955; Phys. Lett. **B278** (1992) 193.

[14] G. A. Schuler and T. Sjöstrand, Z.Phys. **C73** (1997) 677.

[15] A. Donnachie, H. G. Dosch and M. Rueter, Eur. Phys. J. **C13** (2000) 141.

[16] A. Corsetti, R.M. Godbole and G. Pancheri, Phys. Lett. **B435** (1998) 441 and references therein; R. M. Godbole, A. Grau and G. Pancheri, IISC-CTS-7-99, hep-ph/9908220; R. M. Godbole, A. Grau, G. Pancheri, hep-ph/9912395, IISC-CTS-8-99.

[17] A. Donnachie and S. Soldner-Rembold, hep-ph/0001035, FREIBURG-EHEP-2000-01.

[18] E. Gotsman et al., hep-ph/0001080, TAUP-2618-00.

[19] M. Glück, E.Reya and A.Vogt, Phys.Rev. **D46** (1992) 1973.

[20] M. Gluck, E. Reya and I. Schienbein, Phys.Rev. **D60** (1999) 054019.

[21] A. M. Cooper-Sarkar, R. C. E. Devenish and A. De Roeck, Int.J.Mod.Phys. **A13** (1998) 3385.

[22] A. Vogt, Proceedings of the International Conference on the Structure and Interactions of the Photon, PHOTON 99, Freiburg, 1999, Nucl. Phys. Proc. Suppl. **82** (2000) 394; E. Accomando et al., Phys. Rep. **299** (1998) 21.

[23] G. A. Schuler and T. Sjöstrand, Z. Phys. **C68** (1995) 607.

[24] A. Donnachie and P.V. Landshoff, Phys. Lett. **B296** (1992) 227.

[25] PLUTO Collaboration; Ch. Berger et al., Phys. Lett. **B142**, (1984) 111; Nucl. Phys. **B281** 365.

[26] TPC/2γ Collaboration; H. Aihara et.al., Z. Phys. **C34** (1987) 1.

[27] L3 Collaboration; M. Acciarri et al., Phys. Lett. **B 436** (1998) 403.

[28] OPAL Collaboration, Physics Note PN389 (1999).

[29] OPAL Collaboration, K. Ackerstaff et al., Z.Phys. **C74** (1997) 33.

[30] PLUTO Collaboration; Ch. Berger et al., Phys. Lett. **B149** (1984) 421; Z. Phys. **C26** (1984) 353.

[31] TPC/2γ Collaboration; H. Aihara et al., Phys. Rev. **D41** (1990) 2667.

[32] MD-1 Collaboration; S.E. Baru et al., Z. Phys. **C53** (1992) 219.

[33] L3 Collaboration; G. Passaleva, talk presented at the IX Lomonosov Conference on Elementary Particle Physics, Moscow, September 20-26, 1999 (to appear in the proceedings).

[34] OPAL Collaboration; G. Abbiendi et al., CERN-EP/99-076.

[35] DELPHI Collaboration; N. Zimin, Proceedings of the International Conference on the Structure and Interactions of the Photon, PHOTON 99, Freiburg, 1999, Nucl. Phys. Proc. Suppl. **82** (2000) 139.

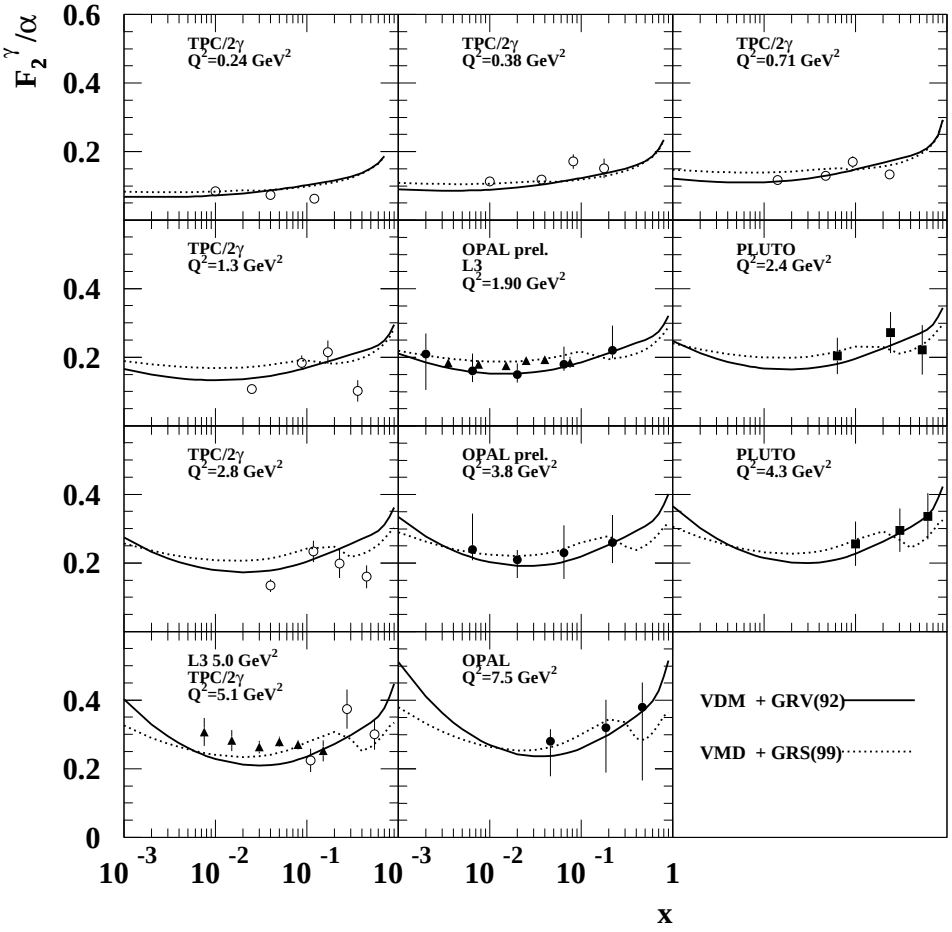

Figure 6: Comparison of our predictions for F_2^γ/α as a function of x for different values of Q^2 in the low Q^2 region, with experimental results [25, 26, 27, 28, 29]. The curves correspond to different LO parametrisations of $F_2^{\rm QCD}/\alpha$: GRV [19] (solid line) and GRS' [20] (dotted line). Error bars correspond to statistical and systematic errors added in quadrature.

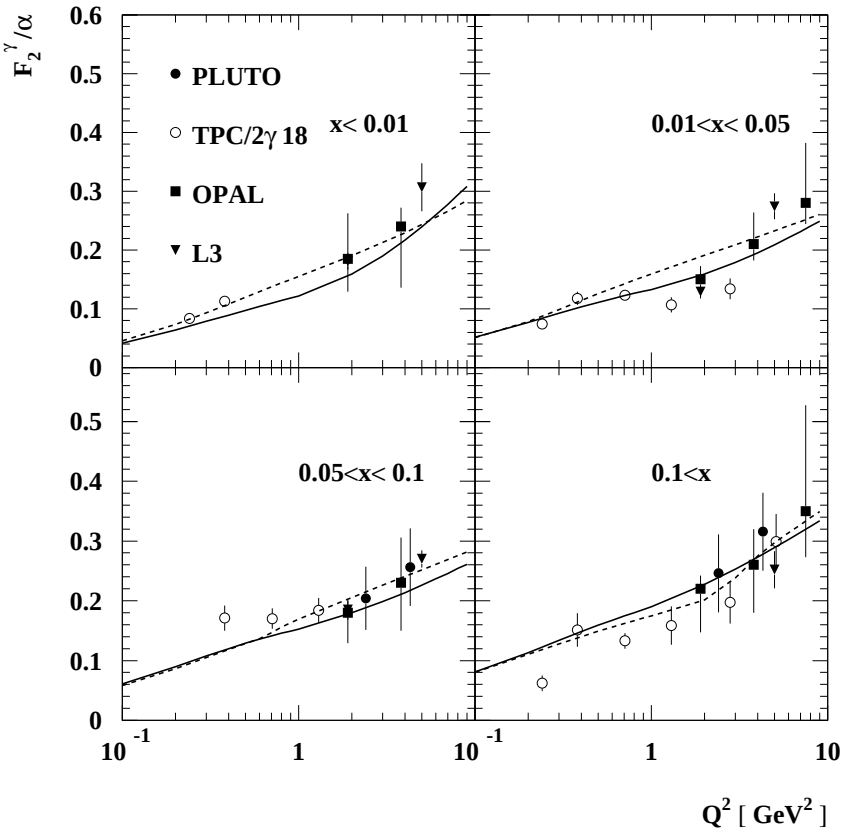

Figure 7: Comparison of our predictions for F_2^γ/α, as a function of Q^2 in the low Q^2 region, for different intervals of x, with experimental results [25, 26, 27, 28, 29]. The curves correspond to different LO parametrisation of $F_2^{\rm QCD}/\alpha$: GRV [19] (solid line) and GRS' [20] (dashed line). Curves are plotted for the following values of x (clockwise): 0.0075, 0.0317, 0.0790 and 0.2617. Error bars correspond to statistical and systematic errors added in quadrature.

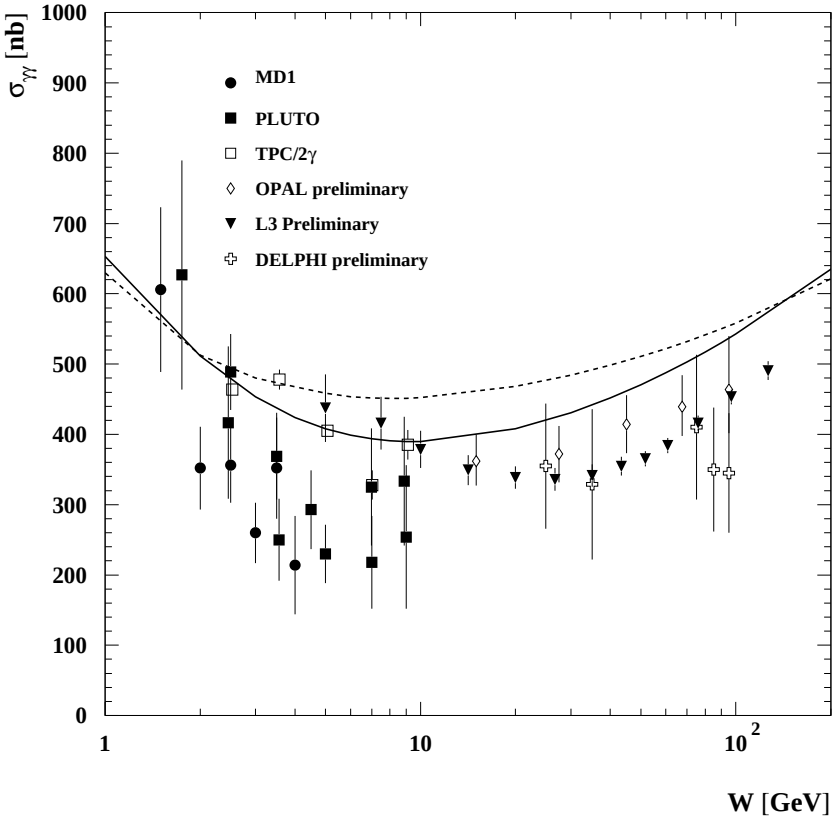

Figure 8: Comparison of our predictions for $\sigma_{\gamma\gamma}(W)$ based on equation (15) with experimental results [30, 31, 32, 33, 34, 35]. The curves correspond to different LO parametrisations of $F_2^{\rm QCD}$: GRV [19] (solid line) and GRS' [20] (dashed line). Error bars correspond to statistical and systematic errors added in quadrature.

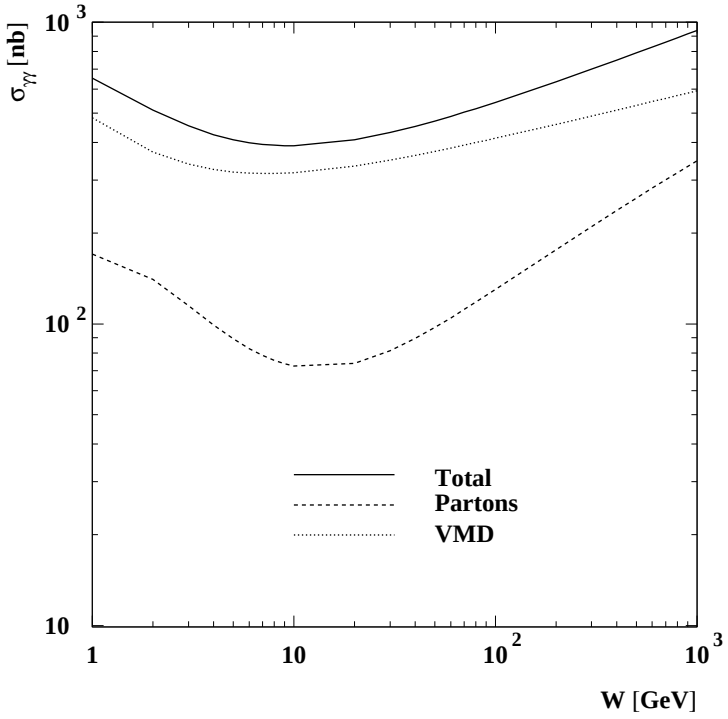

Figure 9: The total $\gamma\gamma$ cross-sections $\sigma_{\gamma\gamma}(W)$ (continuous line) calculated from equation (15) and plotted in a wide energy range which includes the region that will be accessible in future linear colliders. Shown separately are the VMD (dotted line) and partonic (dashed line) components of $\sigma_{\gamma\gamma}(W)$. They correspond to the first and the second term of the r.h.s. of equation (15) respectively. Partonic contribution was obtained using the LO GRV [19] parametrisation of $F_2^{\rm QCD}$

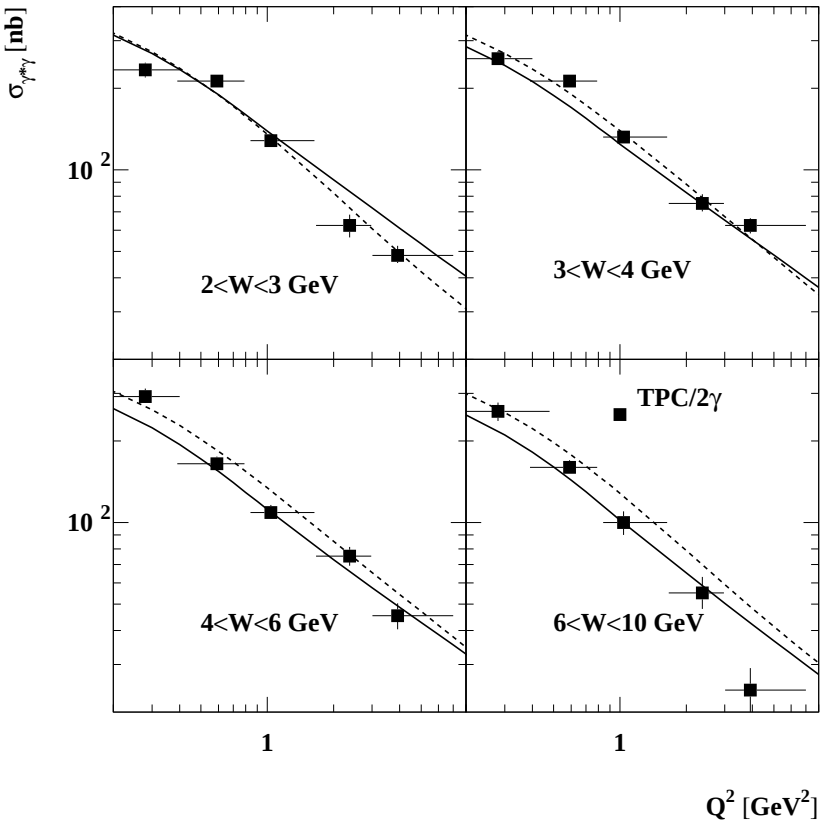

Figure 10: Comparison of predictions for $\sigma_{\gamma^*\gamma}(W, Q^2)$ in the low Q^2 region based on equations (13, 10, 11) and (14) with experimental results [31]. The curves correspond to the LO parametrisations of $F_2^{\rm QCD}$: GRV [19] (solid line) and GRS' [20] (dashed line) respectively. Error bars correspond to statistical and systematic errors added in quadrature.

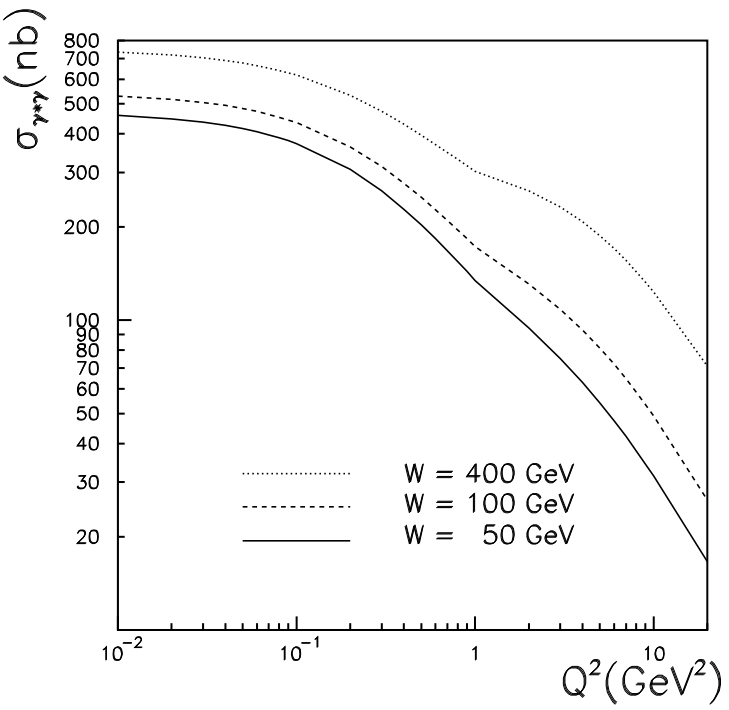

Figure 11: The total $\gamma^*\gamma$ cross-sections $\sigma_{\gamma^*\gamma}(W, Q^2)$ calculated from equation (14) as a function of Q^2 for different values of the centre-of-mass energy W. Partonic contribution was obtained using the LO GRV [19]parametrisation of $F_2^{\rm QCD}$ obtained from GRV [19].